Braz J Phys (2016) 46:56–69
DOI 10.1007/s13538-015-0383-2

SOCIEDADE BRASILEIRA DE FÍSICA

CONDENSED MATTER

Effect of Process Temperature and Reaction Cycle Number on Atomic Layer Deposition of TiO_2 Thin Films Using $TiCl_4$ and H_2O Precursors: Correlation Between Material Properties and Process Environment

W. Chiappim [1,2] · G. E. Testoni [1,2] · J. S. B. de Lima [1] · H. S. Medeiros [2] · Rodrigo Sávio Pessoa [1,2] · K. G. Grigorov [3] · L. Vieira [1,2] · H. S. Maciel [1,2]

Received: 21 July 2015 / Published online: 9 November 2015

Abstract The effect of process temperature and reaction cycle number on atomic layer-deposited TiO_2 thin films onto Si(100) using $TiCl_4$ and H_2O precursors was investigated in order to discuss the correlation between the growth per cycle (GPC), film structure (crystallinity), and surface roughness as well as the dependence of some of these properties with gas phase environment such as HCl by-product. In this work, these correlations were studied for two conditions: (i) process temperatures in the range of 100–500 °C during 1000 reaction cycles and (ii) number of cycles in the range of 100–2000 for a fixed temperature of 250 °C. To investigate the material properties, Rutherford backscattering spectrometry (RBS), grazing incidence X-ray diffraction (GIXRD), and atomic force microscopy (AFM) techniques were used. Mass spectrometry technique was used to investigate the time evolution of gas phase species HCl and H_2O during ALD process. Results indicate that the GPC does not correlate well with film crystallinity and surface roughness for the evaluated process parameters. Basically, the film crystallinity relies solely on grain growth kinetics of the material. This occurs due to higher HCl by-product content during each purge step. Furthermore, for films deposited at variable cycle number, the evolution of film thickness and elemental composition is altered from an initial amorphous structure to a near stoichiometric TiO_{2-x} and, subsequently, becomes fully stoichiometric TiO_2 at 400 cycles or above. At this cycle value, the GIXRD spectrum indicates the formation of (101) anatase orientation.

Keywords Atomic layer deposition · Titanium tetrachloride · Titanium dioxide thin film · Mass spectrometry · RBS · Film crystallinity · Morphology

1 Introduction

The growth of the metal oxide thin film, titanium dioxide (TiO_2), has received a great deal of attention in recent years [1–5]. This is not only due to many important practical applications of TiO_2 thin film but also because it is a valuable object for crystallographic investigations. Basically, the applicability of this material in thin-film form depends on its crystalline structure. As it is known, in bulk form, TiO_2 is a polymorphous material that is known to exist in the main crystalline structures: two tetragonal, the anatase and the rutile phases, and one orthorhombic, the brookite phase. Another orthorhombic structure is the cotunnite TiO_2, which is synthesized at high pressures and is one of the hardest polycrystalline oxide known [3, 6]. However, in thin-film form, only anatase and rutile are easily synthesized [1, 7]. Anatase and rutile phases consist of interconnected TiO_6 octahedral chains that are interconnected in different configurations, resulting in different physical and chemical properties [3, 8]. Due to this,

Authorship Statement The submission of the manuscript has been approved by all coauthors. This manuscript has not been published nor is it currently being considered for publication in any other journal.

✉ Rodrigo Sávio Pessoa
rodrigospessoa@gmail.com

[1] Nanotechnology and Plasmas Processes Laboratory, Universidade do Vale do Paraíba (Univap), Av. Shishima Hifumi, 2911, Urbanova, São José dos Campos, SP 12244-000, Brazil

[2] Plasma and Processes Laboratory, Instituto Tecnológico de Aeronáutica (ITA-DCTA), São José dos Campos, SP 12228-900, Brazil

[3] Space Research and Technology Institute, Acad. G. Bonchev Str. bl.1, 1113 Sofia, Bulgaria

they are potentially attractive in different areas. For example, the high equilibrium temperature rutile phase is desired for optical and microelectronic applications due to its high refractive index and dielectric constant [9]. Anatase phase exhibits high photocatalytic activity, which can be used in a variety of potential applications that include dye-sensitized solar cells, photo-chemically degradation of toxic chemicals, electrode material in lithium batteries, water splitting, and high efficiency photocatalysts [2, 4, 10–12]. Nevertheless, the use of thin films in catalytic applications is limited due to the difficulty in controlling the production of pure-phase anatase TiO_2 and its surface roughness/area. In addition, because anatase TiO_2 is a metastable phase, it begins to transform into rutile phase at high energy processes.

Metal oxide films can be prepared using liquid (sol–gel [13, 14], anodization [15], hydrothermal [16], etc.) and vapor phase deposition methods (sputtering [17, 18], chemical vapor deposition (CVD) [19, 20], and atomic layer deposition (ALD) [21, 22], etc.). Amongst these film growth methods, ALD shows several practical advantages compared to other deposition techniques due to the saturative nature of each reaction step (i.e., the film growth is self-limiting), such as conformal growth, large area uniformity even on profiled substrates, atomic level control of the film thickness and composition, and pinhole free [23, 24].

The ALD of metal oxides typically involves two self-saturating half-reaction cycles, one consisting of a metal precursor such as a halide, metal-organic, or an organometallic, which is followed by exposure of the surface to an oxygen source, such as H_2O, O_3, H_2O_2, or O_2-plasma [24]. In the case of ALD of TiO_2, several titanium precursors have been investigated such as (i) titanium halides, (ii) alkoxides, (iii) alkylamides, (iv) cyclopentadienyls, and (v) heteroleptics [9, 24]. Each precursor group has its limitations, for example the halide titanium tetrachloride ($TiCl_4$) produces HCl, a corrosive by-product, which stimulates additional adsorption or desorption reactions (depending on the process temperature) during film growth process [25], while organometallic precursors tend to decompose at temperatures higher than 300 °C, leading to parasitic CVD-like reactions [26, 27]. However, due to its thermal stability and low cost, $TiCl_4$ is still the most commonly employed titanium precursor [24, 28]. For thermal ALD mode, H_2O is the most common oxygen source for most of the abovementioned titanium precursors.

Although there have been several studies about ALD of TiO_2 from $TiCl_4$ and H_2O precursors, where the majority are focused on applications, the synergistic details of the nucleation, growth kinetics, and crystallization/film structure evolution are not yet well understood, mainly due to lack of correlation between process parameters and experimental results. Table 1 presents, in chronological order, the main advances in these topics. The research on the aforementioned context was initiated in 1993 by Ritala et al. [29, 30], who first investigated the effect of process parameters such as substrate type and process temperature on growth rate and film crystallization. In this work, they observed that TiO_2 film growth on amorphous substrate remained amorphous even at growth temperatures as high as 600 °C. They also proposed a first chemistry pathway to explain the TiO_2 film formation by ALD method. In 1995, Aarik et al. initiated their studies with ALD TiO_2, which focused on investigating the structure and morphology of the as-deposited thin films [31]. They determined the temperature range to obtain amorphous, pure anatase and anatase/rutile TiO_2 on some substrate types (Table 1). Furthermore, they demonstrated that films of certain crystal structure can be grown on amorphous as well as on crystalline substrates under appropriate growth conditions. Finally, they first observed that the crystallinity of TiO_2 film can be dependent on substrate surface roughness. In 2000, Aarik et al. showed the nonlinear behavior of TiO_2 ALD growth rate (or growth per cycle (GPC)) and film roughness with process temperature [35]. At temperatures generally lower than 200 °C, the ALD TiO_2 film tends to be amorphous, and chemistry studies by Aarik et al. correlated this effect with the amount of chlorine adsorbed in film bulk, allowing them to describe a more realistic chemistry pathway for TiO_2 deposition from $TiCl_4$ and H_2O [36]. Another interesting result was presented in 2003 by Mitchell and coworkers from TEM studies, where they verified that films grown on RCA and HF treated silicon have different nucleation modes for crystalline growth [38]. From these works until the recent years, little has been discussed about the chemistry and physics of the $TiCl_4$ and H_2O ALD process. However, in 2008, the work of Cheng and Chen brought new insight concerning the TiO_2 ALD mechanisms [41]. They showed that it is possible to obtain a real ALD process window for TiO_2 growth from $TiCl_4$ and H_2O precursors by only inserting a pump-down step between precursors and purge steps. Additionally, the film structure and morphology behavior with temperature are close to the results of Aarik et al. [35]. Recently, Puurunen et al. presented the effect of ALD process parameters (substrate type, number of cycles, and temperature) on crystallite size and RMS roughness. From these experimental results, they proposed a simplified scheme for the growth of crystalline ALD TiO_2 [42].

Concerning the experimental conditions and main results presented in Table 1, some points deserve considerations: (i) Most of the research usually uses different substrates and ranges of ALD process parameters, thus making the comprehensive analysis of the effect of external parameters on the characteristics of ALD TiO_2 films difficult; (ii) in this sense, there is a discrepancy between the experimental data of different authors, even when the same substrate type was used; (iii) and finally, although the TiO_2 ALD process is well studied, especially in the context of applications, there are little data in the literature that correlates and explains the dependence of the film structure (crystallinity) with other properties

Table 1 Evolution of ALD TiO_2 research using $TiCl_4$ and H_2O as precursors on film structure, chemistry, and morphology

Process temperature (°C)	Substrate type	ALD cycle steps/process pressure	Main results	Reference
150–600	Soda lime glass, corning 1733, amorphous Al_2O_3 layer on soda lime glass, polycrystalline Al_2O_3, silicon	0.2/0.5/0.2/0.5 s[a] 10 mbar	- Growth temperature, number of cycles and substrate type effect on the growth rate. - Crystallinity: on amorphous substrates films were amorphous, but on crystalline substrates they were crystalline and partially oriented.	[29]
500	Mica, soda lime glass	0.2/0.5/0.2/0.5 s[a] 10 mbar	- No remarkable differences in the morphology between crystalline and amorphous films were observed. - TiO_2 surface roughness increased with film thickness.	[30]
100–500	Soda lime glass, fused silica, silicon (111)	2/1/1/2 s[a] 2.5 mbar	- Amorphous films grew at temperatures below 165 °C, anatase structure was observed in the films grown at 165–350 °C while rutile dominated in the films obtained at temperatures above 350 °C. - High surface roughness was observed at the temperature of amorphous to crystalline phase transition.	[31]
400	Silicon (111)	2/1/1/2 s[a] 2.5 mbar	- Investigate the structure of TiO_2 films grown at different water vapor pressures. - Higher water vapor pressures (≥0.02 mbar) allow to achieve rutile phase.	[32]
100–400	Fused silica, silicon (111)	2/1/1/2 s[a] 2.5 mbar	- Dependence of Ti/O ratio on the growth temperature is very weak. - Chlorine contamination significantly decreases with increasing deposition temperature.	[33]
150	Mica, GaAs (100), fused silica	0.2/0.5/5/10 s[a] not informed	- Appearance of anatase inclusions in the amorphous base layer of TiO_2.	[34]
100–425	Mica, GaAs (100), fused silica	Variable[a] 2.5 mbar	- Structural studies revealed that the surface roughening and growth rate were connected with crystallization. - The growth rate and roughness presents a nonlinear behavior with process temperature.	[35]
100–400	Single crystal (100)-oriented silicon, amorphous silica	Variable[a] 2.5 mbar	- Low growth rate which was obtained in the $TiCl_4/H_2O$ ALD process was found to be a result of a significant chlorine amount adsorbed during the $TiCl_4$ pulse. - A detailed mechanism of film growth is presented.	[36]
100–400	Amorphous silica, single crystal Si(100), α-Al_2O_3	Variable[a] 2.5 mbar	- Deposition of crystalline TiO_2 in amorphous substrate.	[37]
250–350	Silicon (100)	0.3/0.5/0.4/0.5[a] 10 mbar	- Comparison of films grown on RCA treated silicon and HF treated silicon has shown very different nucleation modes for crystalline growth.	[38]
300	Silicon (100)	0.3/0.5/0.4/0.5[a] not informed	- The morphology of the films is dependent on the nature of the initial surface.	[39]
125–680	Fused silica, single-crystal silicon, sapphire	Variable[a] 2.5 mbar	- Raman structural analysis of TiO_2 thin films in different substrates.	[40]
200–500	N-type silicon (100)	1 s per step[b] 0.4 mbar in deposition/ 0.27 in pump-down	- A nondependent process temperature growth rate during TiO_2 ALD deposition was achieved inserting a pump-down step between precursors and purge steps.	[41]
110–300	Thermal SiO_2, RCA-cleaned Si, ALD Al_2O_3	0.1/4/0.1/4 s[a] 0.4 mbar	- Effect of process parameters (substrate type, number of cycles and temperature) on crystallite size and RMS roughness. - Scheme for the growth of crystalline ALD TiO_2.	[42]
125–500	Silicon (100)	0.5/2/2/5 s[a] 2.2–2.4 mbar	- A comparison between $TiCl_4$–H_2O and a hydrogen-free precursors $TiCl_4$–O_3 ALD process is presented. - Effect of process temperature on surface roughness. It was observed a drastic increase of surface roughness for temperatures higher than 400 °C.	[43]

[a] $TiCl_4$ reactant, N_2 purge, H_2O reactant, and N_2 purge

[b] $TiCl_4$ reactant, pump-down, Ar purge, pump-down, H_2O reactant, pump-down, Ar purge, and pump-down

such as composition and morphology, when parameters such as process temperature and cycle number are varied.

In this perspective, this work presents studies concerning the effect of process temperature and cycle number on atomic layer deposited TiO_2 thin films using $TiCl_4$ and H_2O precursors in order to discuss the correlation between the GPC, film structure (crystallinity), and surface roughness as well as the dependence of some these properties with process environment. In order to correlate with the main literature of this area and also to complement most of the observations presented thus far, all investigations were done with the most common substrate in literature about wide band gap materials: silicon. To investigate the material properties, Rutherford backscattering spectrometry (RBS), grazing incidence X-ray diffraction (GIXRD), and atomic force microscopy (AFM) techniques were used. Mass spectrometry technique was used to investigate the time evolution of gas phase species HCl and H_2O during ALD process.

2 Experimental

2.1 Film Growth

Pieces of silicon wafer (500 μm thick, p-type, 5×10^{-3} Ω cm, (100)-orientation) were used as substrates. The substrates were individually cleaned in an ultrasonic bath using acetone and deionized water for 5 min, and then, they were dried with nitrogen gas before introduction into the reaction chamber. TiO_2 films were deposited by a TFS-200 ALD system from Beneq operating in thermal mode. Here, the following ALD cycle time steps for film deposition were used: 0.25–2–0.25–2 s, i.e., the $TiCl_4$ pulse of 0.25 s, the first purge of 2 s, H_2O pulse of 0.25 s, and the second purge of 2 s. Nitrogen (N_2) of 99.999 % purity was used as purge gas. The vapors of $TiCl_4$ and H_2O were led into the reaction chamber from external reservoirs kept with liquid $TiCl_4$ (Sigma-Aldrich, 99.95 % purity) and deionized water at temperature of 21 °C. A capillary tube, adapted to the reactor, was used to control the precursor flow injected into the ALD chamber, by action only of the precursor vapor pressure, i.e., no bubbling system was used. The base pressure of the reactor was lower than 10^{-2} mbar and during the deposition, and the gas pressure was maintained around 1.0 mbar through the insertion of 300 sccm of N_2.

In this work, the ALD TiO_2 films were deposited for two conditions: (i) process temperatures in the range 100–500 °C during 1000 reaction cycles and (ii) number of cycles in the range 100–2000 for a fixed temperature of 250 °C. The variation of the substrate temperature did not exceed 3 °C for all conditions investigated.

2.2 Film Characterization

Rutherford backscattering spectroscopy (RBS) was used to measure the thickness and chemical composition of the film. Measurements were carried out using a 2.2 MeV $^4He^+$ beam from a Pelletron type accelerator with a particle detector positioned at 170° to the incident beam. For data evaluation of the RBS spectra, the computer code SIMNRA [44] was used taking into account the electronic stopping power data by Ziegler and Biersack, Chu+Yang's theory for electronic energy-loss straggling, and Andersen's screening function to Rutherford cross section. The contribution from a multiple scattering into the RBS spectra was taken into account using the calculating facilities of SIMNRA. For all investigated films, the simulated RBS areal density values (10^{15} atoms/cm^2) were converted into the layer thickness value (nm) by using the theoretical TiO_2 density, taking into account the crystal structure of the as-deposited material.

In order to verify the accuracy of thickness measurements, one sample was analyzed by transmission electron microscopy (TEM) using a JEOL JEM2100F with EELS Gatan Tridium and EDS Thermo-Noran (the substrate was prepared by tripod polishing). Figure 1a, b shows the cross section TEM image of interface between Si substrate and TiO_2 thin film deposited at condition of 250 °C and 1000 cycles. The film thickness measured by TEM was 82.3 nm (Fig. 1a), while RBS was 83.0 nm. Moreover, Fig. 1b shows the 2.7 nm thick natural SiO_2 layer between TiO_2 and Si. Figure 1c shows that the TiO_2 film composition is uniform along the film depth. Our data (e.g., Fig. 1b) and others works [36, 40] show that the initial stages of TiO_2 film growth in temperatures higher than 200 °C involve the formation of an amorphous layer, which subsequently crystallizes for more cycles.

In order to characterize the crystal structure, grazing incidence X-ray diffraction (GIXRD) method was used. The GIXRD patterns were obtained at room temperature in a Shimadzu XRD 6000 goniometer using copper target (CuK_α radiation 1.5418 Å), 2θ from 10° to 80°, at a scanning speed of 0.02°/s, a voltage of 40 kV, and a current of 30 mA. Additionally, the GIXRD studies were carried out at an incidence angle of 0.29°. This angle was close to the optimum values for analysis of anatase and rutile films and allowed efficient reduction of the reflections from the substrate [43].

The morphological images were obtained using a multimode atomic force microscope (AFM) from Bruker. The studies were carried out in air using Si cantilevers with a typical tip radius ≤10 nm, and data were collected from a surface area of 1×1 μm^2. During the slide, mechanical oscillation of the probe was monitored by four photodetector quadrants and was analyzed using two feedback loops. The first loop controlled the distance between the tip and the sample, while the second feedback loop adjusts the tip-sample separation to maintain constant amplitude and force on the sample. Thus,

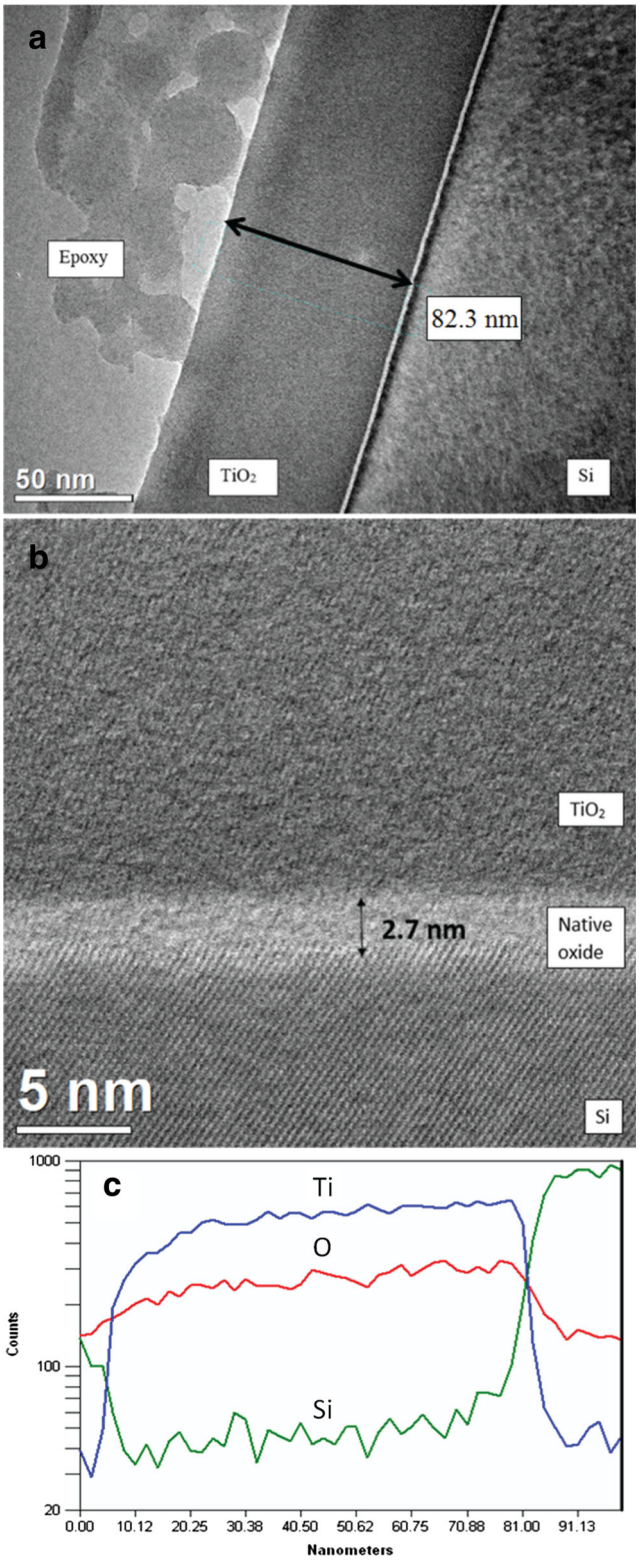

Fig. 1 **a** TEM image of ALD TiO_2 film on Si(100) substrate deposited at condition of 250 °C and 1000 cycles. **b** TEM image in brightfield of interface between Si(100) substrate and TiO_2 thin film. **c** TiO_2 film composition along film depth

the tip scanned the surface at constant oscillation amplitude in a tapping mode. This method of "tapping" lessens the damage done to the surface and has been used to solve a problem of high lateral forces observed in contact mode between the cantilever and surface but still maintaining very high lateral resolution. The lateral contribution is reduced because the tip touches the surface only for a short time, thus avoiding the issue of lateral forces and drag across the surface. Contrast images were computer decoded and recorded using gold-scale. The AFM images and root mean squared (RMS) surface roughness were treated by Gwyddion data analysis software [45].

2.3 Gas Phase Analysis: Mass Spectrometry Technique

The analysis of the partial pressure of the species extracted from the gas phase was performed by using a mass spectrometer from Stanford Research Systems (RGA-200), which allows analysis of mass up to 200 atomic mass unit (amu) with a resolution of 1 amu, adapted to the exhaust of the process chamber. The residual species were sampled through a micro orifice located at the entrance of the mass spectrometer and underwent subsequent electron impact ionization at constant electron energy of 70 eV. This energy is sufficient to ionize the neutral gas species that enter through the quadrupole RF mass filter and thus are detected and classified as a function of their mass-to-charge ratio. The typical operation pressure within the mass spectrometer was 10^{-6} mbar.

3 Results and Discussion

3.1 Effect of Process Temperature

As frequently presented in literature, the GPC is a main parameter to be evaluated in ALD processes. Figure 2 presents the GPC of ALD TiO_2 thin films on Si(100) as a function of process temperature, where the results of the present work and, for comparison, some results from literature are shown [35, 41, 42].

The average monolayer thickness, $\overline{h}^{ml}$ (nm), is given from Eq. 1 [23]:

$$\overline{h}^{ml} = \left(\frac{M}{\rho N_A}\right)^{1/3} \tag{1}$$

where M is the molar mass (M_{TiO2}=79.67 g mol^{-1}), ρ is the density of the material ($\rho_{amorphous}$=3.59×10^{-21} g nm^{-3}, $\rho_{anatase}$=3.77×10^{-21} g nm^{-3}, and ρ_{rutile}=4.13×10^{-21} g nm^{-3} [23]), and N_A is the Avogadro constant (6.02214×10^{23} mol^{-1}). Thus, one monolayer of amorphous TiO_2 is 0.333 nm, anatase 0.325 nm, and rutile 0.315 nm thick. Comparing with Fig. 2, the GPC for temperature range of 100–500 °C corresponds about 13–34 % of a monolayer. This occurs due to saturation of the surface with adsorbed

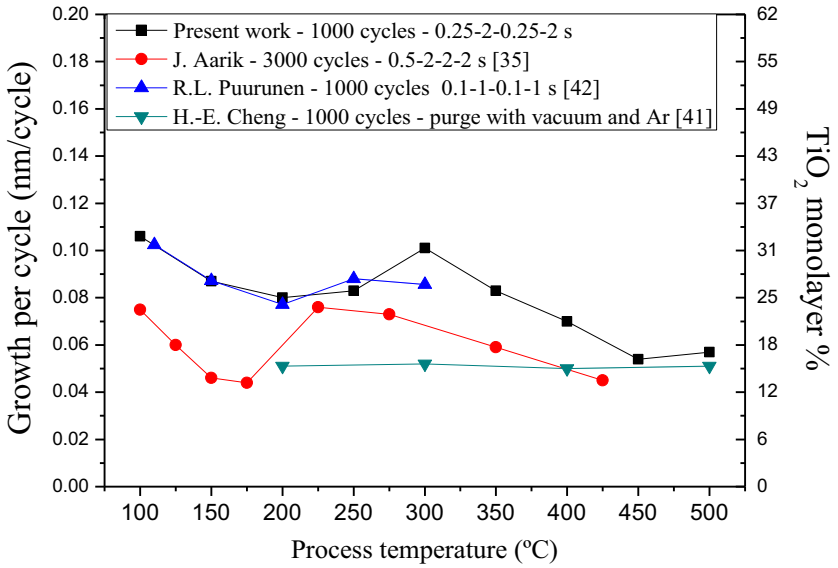

Fig. 2 Growth per cycle of ALD TiO_2 thin films on Si as a function of process temperature. The ALD cycles presented in text box are relative to $TiCl_4$ reactant, N_2 purge, H_2O reactant, and N_2 purge

species in a self-terminating gas–solid reaction. Two factors contribute for saturation: steric hindrance of the ligands and the number of reactive surface sites [23]. Steric hindrance of the ligands can cause the ligands of the chemisorbed species to shield part of the surface from being accessible to the reactant. The surface can be considered "full." The number of bonding sites on the surface may also be less than that required for achieving the maximum ligand coverage. In that case, although space remains available on the surface, no bonding sites are accessible. Because of these factors, the GPC, in ALD from compound reactants, should be considerably less than a monolayer of the ALD-grown material.

Another important observation from Fig. 2 concerns the nonlinear behavior of GPC with process temperature ranging from 175 to 350 °C (also referred to as anomalous effect of GPC [35]). As can be seen, it occurs for various conditions of metal or ligand precursor pulse and cycle number. The work of Cheng and Chen [41] is the only one where the cycle performed by a pump-down between each step (see Table 1) allows the achievement of a GPC independent of the process temperature. This behavior indicates that the reaction is overall self-limited by the saturated surface adsorption of reactants, and consequently, the adsorption rate is almost the same along the whole range of temperatures investigated. Comparing our present results with those of Cheng and Chen, both obtained at 1000 cycles, it is feasible to infer that when the nonlinear behavior of GPC with process temperature occurs, the TiO_2 growth-mode is not self-limited. A possible explanation for this could be attributed to probable overlapping between metallic and ligand precursors during purge times, causing the appearance of CVD-like reactions [46–48] and/or inefficient draining of the by-products (such as hydrogen chloride, HCl) after each half-reaction step [25]. Elers et al. showed that for trimethylaluminium (TMA) precursor, at 270 °C, N_2 purge times in the order of 27 s (flow rate=100–200 sccm) were necessary to remove the excess TMA from the source delivery line [48]. As the purge times for most of the ALD TiO_2 works are from 0.5 to 2.0 s (Table 1), these periods are probably insufficient to remove all $TiCl_4$, H_2O, and by-product species from reactor and/or source delivery line prior to precursor insertion. Recent work of Leem and coworkers showed that the presence of HCl after the first and/or second half-reaction steps can influence the GPC of TiO_2 thin films [25].

In order to observe the HCl variation during each half-reaction, mass spectrometry measurements of the partial pressure of HCl^+ species (mass 36) were performed during first cycles of ALD process as shown in Fig. 3. The partial pressure of H_2O^+ species (mass 18) was also tracked in order to observe the second half-reaction step and the purge efficiency of this species during deposition process. According to Fig. 3a–c, an increase of partial pressure of HCl^+ in the first reaction cycles was observed, and with increase of deposition time, this tends to saturate. Moreover, the HCl^+ partial pressure was strongly dependent on process temperature. Meanwhile, the partial pressure of H_2O^+ species underwent a short variation with deposition time for all investigated temperatures. We can conclude that the purge time of 2.0 s after each half-reaction step is not sufficient to remove H_2O and HCl molecules and probably $TiCl_4$ species (not analyzed here due to low intensity in mass spectrometer). This fact does not occur if longer cycle time steps are considered. Figure 3d–f presents the HCl^+ and H_2O^+ partial pressure variation with deposition time when the cycle time steps are multiplied by 10, i.e., $TiCl_4$ pulse of 2.5 s, the first purge of 20.0 s, H_2O pulse of 2.5 s, and the second purge of 20.0 s, for process temperatures of 100, 250, and 300 °C, respectively. As shown in Fig. 3d–f, for longer time steps, there is sufficient time to remove the HCl during each half-reaction step. This effect becomes more evident at high

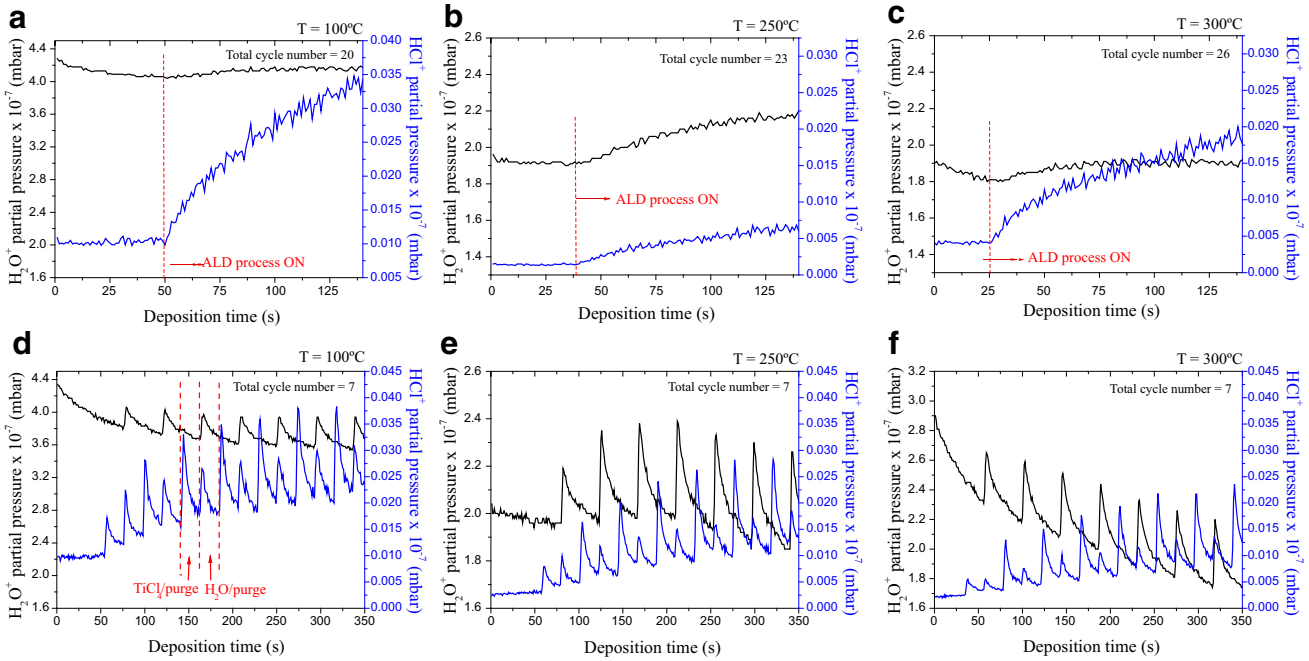

Fig. 3 Partial pressure time evolution of HCl^+ and H_2O^+ species for cycle time steps of 0.25–2–0.25–2 s (**a**–**c**) and 2.5–20–2.5–20 s (**d**–**f**), for process temperatures of 100, 250, and 300 °C

process temperatures. Concerning the H_2O purge, an efficient reduction of partial pressure of H_2O^+ after water pulse was observed, a fact that results in a steady decrease of the H_2O^+ partial pressure during the first process cycles. This was not observed for the case of purge time of 2.0 s (see Fig. 3a–c). Our mass spectrometry analysis agrees with the results of Elers et al., showing that longer purge time steps are necessary to remove the precursors as well as by-products, consequently reducing the overlapping of the precursors. However, the time spent for total cycle time is longer, and for actual industry process requirements, it is not a good alternative. In Cheng and Chen work, the precursor overlapping was overcome by shorter pump-down steps after each step of the total cycle. This pump-down step was also checked by Elers et al. for TMA, and a considerable reduction of purge time was achieved [48].

Still in Fig. 3, it is important to emphasize the effect of process temperature on kinetics of HCl and H_2O species. Note that H_2O^+ partial pressure is directly dependent on process temperature, where for high temperatures, it tends to reduce due to high reactivity with $(–O–)_nTiCl_{4-n}$ radicals, n=1–3, formed on substrate/reactor wall surface [25]. This H_2O^+ partial pressure variation with temperature was the same for both cycle time steps evaluated. However, the main by-product after each half-reaction, the HCl, does not show the same behavior with temperature when cycle time steps are compared. For the case of the precursor cycle time investigated in this work, 0.25 s, the HCl^+ partial pressure increased to 150 °C, decreased to 250 °C, and increased again to 300 °C (Fig. 3a, b). On the other hand, for the case of precursor cycle time of 2.5 s, a constant decrease of the HCl^+ partial pressure with process temperature was observed (Fig. 3d–f). Comparing the tendency of the partial pressure of HCl^+ in Fig. 3a–c with our results in Fig. 2, it can be inferred that the HCl^+ species is a good indicator of the behavior of GPC when the process temperature is varied.

Regarding ALD TiO_2 film structure, Fig. 4a, b shows GIXRD spectra of TiO_2 films grown at temperatures ranging from 100 to 500 °C. At temperatures in the range 100–200 °C, the TiO_2 film is amorphous, while for temperatures in the range of 250–500 °C, the formation and predominance of anatase phase were observed. Comparing the results of Figs. 2 and 4a, b, for temperatures in the range of 100–200 °C, some literature evidences can be highlighted for GPC decrease and resulting amorphous film: (1) higher chlorine concentration in TiO_2 film bulk for low process temperature (see Fig. 5 and references [33, 37]), (2) decrease of surface OH group concentration with increasing temperature [25, 46], and (3) the lower activity for nucleation rate at low process temperature [50]. On the other hand, when deposition process achieves a critical "activation temperature," some points of the growing film begin to evolve into "agglomerates" of ordered material (nanocrystalline parts), which initiates its crystallization according to the pathway nucleation theory [50]. At this critical temperature (the literature indicated that, depending on process parameters, it can be between 160 and 225 °C), the crystallinity of the TiO_2 film is drastically increased. This can be better observed by comparing Figs. 2 and 4c, where the latter presents the main anatase diffraction peaks (101), (004), (220), and (211) as a function

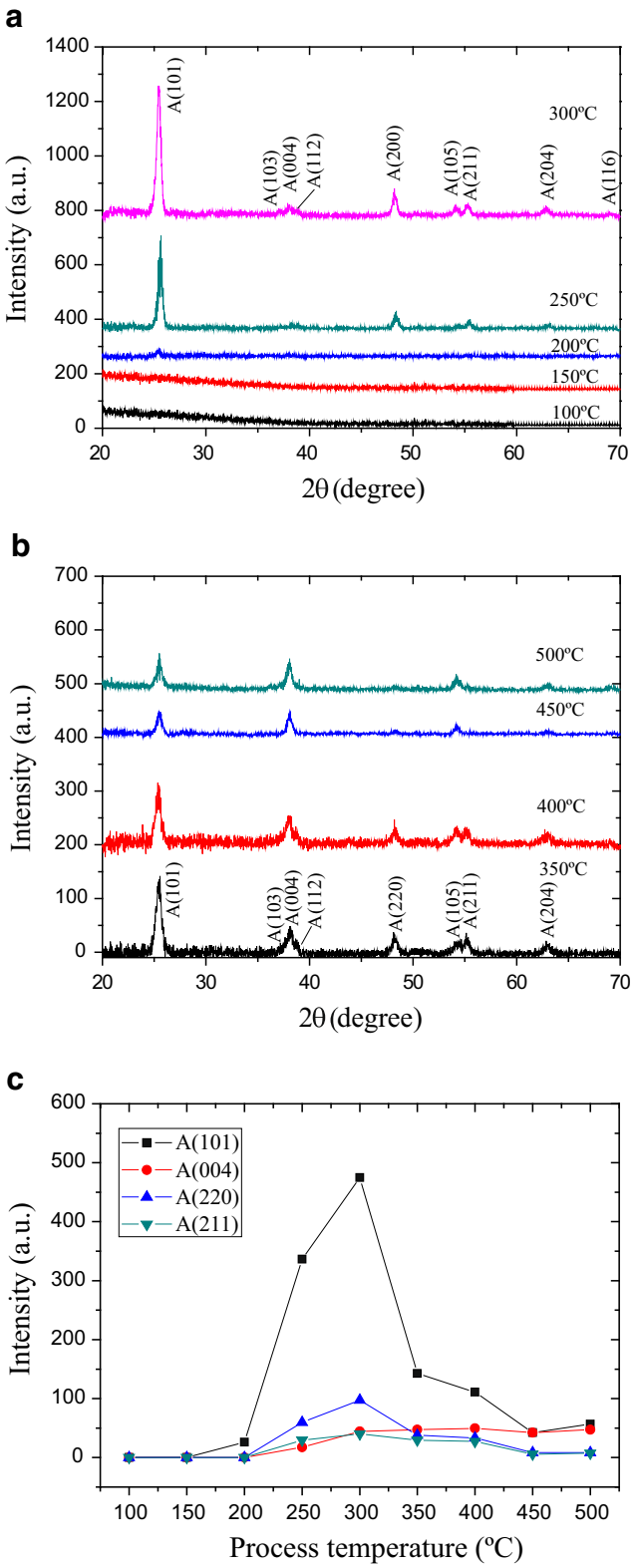

Fig. 4 **a** GIXRD spectra as a function of process temperature. **b** Variation of main anatase peaks intensity as a function of process temperature. Curves have been shifted vertically for clarity. For comparison, the relative intensities of X-ray reference diffractions of anatase powder are (101)/100, (200)/35, (004)/20, (105)/20, (211)/20, (204)/14, (103)/10, (112)/10, (116)/6, and (213)/4 [49]

of process temperature. At temperature of about 300 °C, the film crystallinity reaches a maximum, and from this, value begins to decrease until stabilizing for temperatures from 400 to 500 °C. Concomitantly, in our and cited literature results, the GPC also follows this behavior. Note that the maximum value of the GPC is reached for temperatures in the range of 225–300 °C for the works presented in Fig. 2.

An interesting point to be stressed from the work of Cheng and Chen [41] is concerning the XRD spectra measured between 200 and 500 °C. They present a similar behavior to that observed for anomalous effect of GPC, indicating that when the crystallization process is initiated, the correlation with GPC is lost. Based on this, it is necessary to correlate the film crystallinity with other parameters of the as-deposited film such as surface roughness and grain size [34].

Figure 6 illustrates the AFM images of surface morphology of the TiO_2 thin films deposited at process temperature ranging from 100 to 400 °C. Additionally, Fig. 7 shows the root mean square (RMS) surface roughness of ALD TiO_2 films as a function of process temperature measured in this work (data in black) and from other works of literature [35, 43]. Noticeably, the dependence of RMS surface roughness with process temperature was quite similar to that observed for the diffraction peaks of TiO_2 in Fig. 4, confirming the connection between the crystallinity and surface roughness, and consequently, the grain size. As can be seen from data in Figs. 6 and 7, the grain size and RMS surface roughness are maximum at temperatures in the range of 175–300 °C. Similar results are also observed in references [36–38, 41], but in different

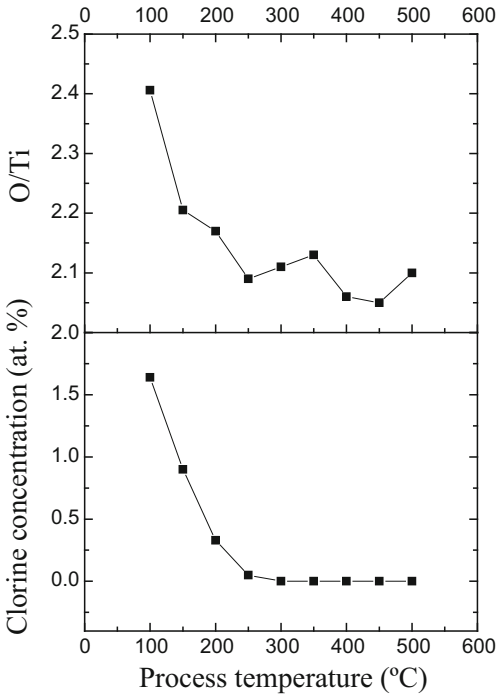

Fig. 5 Chlorine atomic percentage and O/Ti ratio in ALD TiO_2 thin film as a function of process temperature

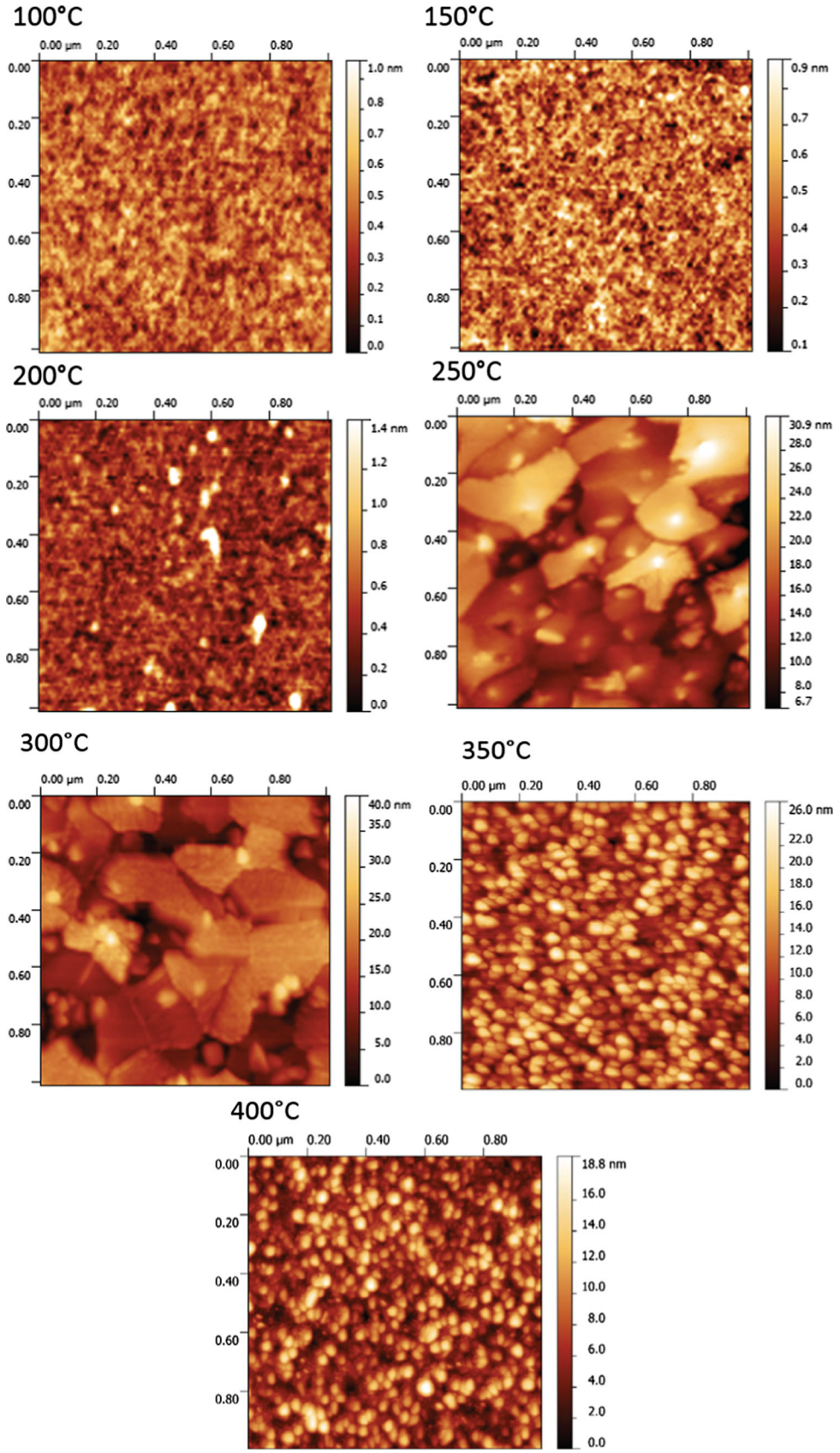

Fig. 6 AFM images of ALD TiO_2 thin films as a function of process temperature for fixed condition of 1000 growth cycles

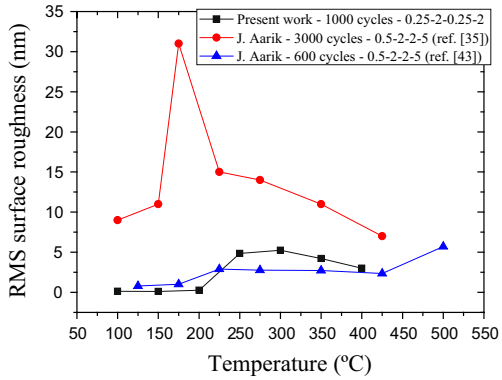

Fig. 7 RMS roughness of ALD TiO_2 thin films as a function of process temperature determined from AFM images of Fig. 6

growth conditions, where the most pronounced effect was caused by the number of reaction cycles. In fact, as the cycle number is augmented, the film thickness and the effect of coalescence of the grains also increase. Although in the work of Cheng and Chen, the TiO_2 surface roughness was not quantified, it is possible to see from the SEM images of their work that the grain size increases for temperatures higher than 200 °C and, subsequently, decreases for temperatures higher than 300 °C. Only for temperature of 500 °C, the grain size again enlarges, possibly due to change of TiO_2 structure, consisting of a mix of anatase/rutile phases [41]. Analysis of Figs. 4c and 7 observed that when TiO_2 film becomes crystalline, both GPC cases (anomalous and constant behavior with temperature) are in agreement with the pathway nucleation theory, which is usually accepted to explain the correlation between crystallinity and grain size when the temperature is increased. Basically, the nucleation pathway establishes that at a certain degree of supersaturation, crystal growth tends to proceed along its adjacent crystal phases, step by step, toward anatase phase because the nucleation barrier of anatase TiO_2 (the difference between the free energy of a generic phase up to the anatase phase) is higher than those of the adjacent phases (the difference between the free energy of a generic phase up to the amorphous film) [50].

Finally, it was observed from RBS results (Fig. 5) that the composition of the ALD TiO_2 film becomes near stoichiometric when it starts to crystallize, indicating that there is a strong dependence between composition and structure of ALD TiO_2 material growth from $TiCl_4$ and H_2O precursors.

3.2 Effect of Reaction Cycle Number

The thickness and GPC of TiO_2 films as a function of reaction cycle number are shown in Fig. 8a, b, respectively. As presented in ALD literature for other oxides such as Al_2O_3 and HfO_2 [23, 51] and in Fig. 8a, there is a linear relationship of ALD film thickness with cycle number. For TiO_2, the works that present these results are [38, 42, 52–54]. The slope of

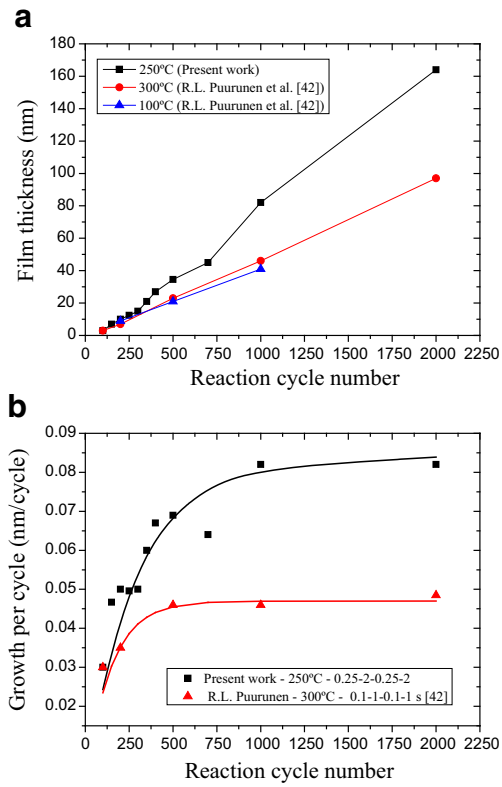

Fig. 8 **a** Film thickness and **b** growth per cycle of ALD TiO_2 thin films as a function of cycle number

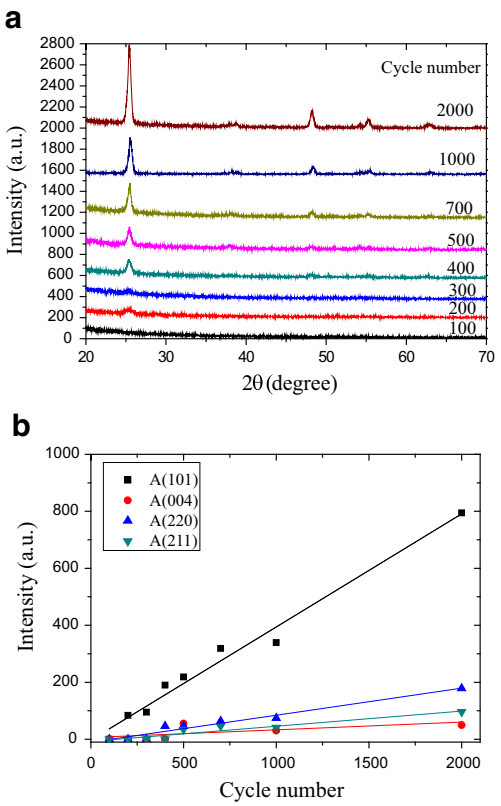

Fig. 9 **a** GIXRD spectra and **b** variation of main anatase peak intensity as a function of cycle number. Curves have been shifted vertically for clarity

curve is dependent on process temperature and precursor time step. On the other hand, the GPC as a function of cycle number (Fig. 8b) has a sharp increase, and at a given cycle number, it saturates. The increase of GPC with reaction cycle number most likely originates from the fact that the number of reactive surface sites increases with the number of cycles and this occurs because concomitantly, the composition of the surface also changes [48]. The GPC characteristic curve presented in Fig. 8b is classified as "substrate-inhibited growth type I" [48]. This can be explained considering that the $TiCl_4$ molecules react with OH terminations of ultrathin SiO_2 layer formed in silicon substrate.

Figure 9a presents the GIXRD spectra for different reaction cycle numbers. Initially, up to a thickness of 10 nm, the TiO_2 film is amorphous, confirming the predictions of the literature [36, 40]. Beyond this thickness, the A(101) orientation begins to emerge and from 400 cycles (~27.0 nm); also other orientations appear: A(220), A(211), and A(204). From 1000 reaction cycles (85.0 nm), all orientations of anatase phase are present in GIXRD pattern. To better illustrate this, the main crystallographic orientations of anatase TiO_2 are shown in Fig. 9b as a function of reaction cycle number. Again, the GPC does not follow the crystalline behavior, when the cycle number is varied.

Figure 10 shows the surface morphologies of the TiO_2 thin films deposited on Si(100) substrates for different cycle number at process temperature of 250 °C. Additionally, Fig. 11 presents the RMS surface roughness of the films as a function of cycle number determined from AFM images of Fig. 9. The drastic change in the grain size between 400 and 500 cycles is directly connected to the phase change observed in GIXRD spectra. On the other hand, the increase of reaction cycle number

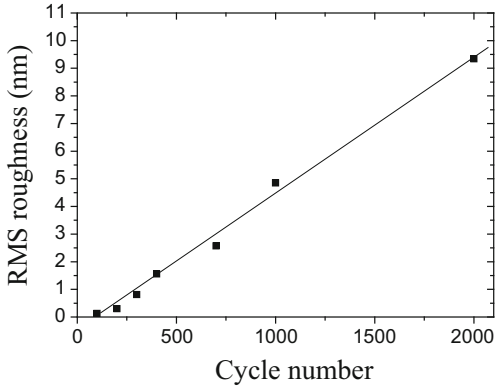

Fig. 11 RMS surface roughness as a function of cycle number. The data was determined from AFM images of Fig. 10

promotes a linear increase in RMS surface roughness of TiO_2 film. Thus, comparing the GPC (Fig. 8b), the main anatase crystallographic orientations (Fig. 9b) and RMS surface roughness (Fig. 11) as a function of reaction cycle number, it is possible to confirm the same behavior between the crystalline evolution and surface roughness of the growing film.

Finally, regarding the evolution of the film composition with cycle number for 250 °C, the RBS spectra for different cycle numbers are illustrated in Fig. 12. As can be seen, in the early stage of growing, the TiO_2 film has low oxygen concentration, becoming stoichiometric only from 400 cycles. Although the RBS analysis has a depth resolution in the order of 5 nm, our results are consistent with the results of reference [50] which show that the TiO_2 film is initially formed with a considerable deficiency of oxygen atoms, a fact that consequently influences the crystallinity during the first steps of film growth.

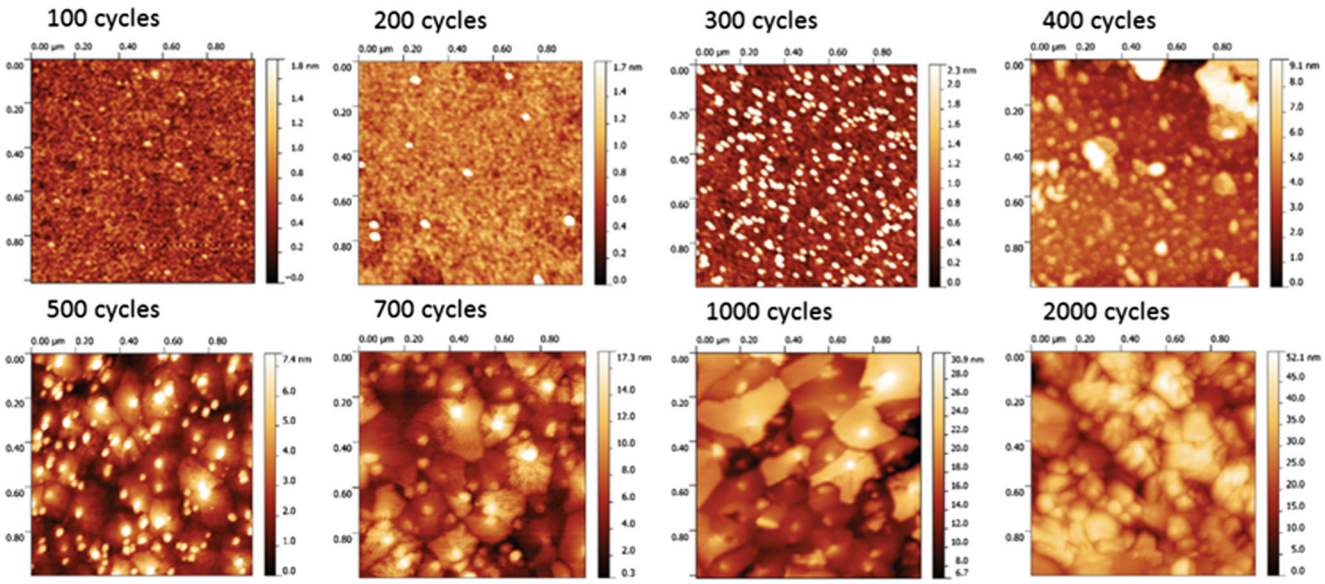

Fig. 10 AFM images of ALD TiO_2 thin films as a function of growth cycle number for a fixed process temperature of 250 °C

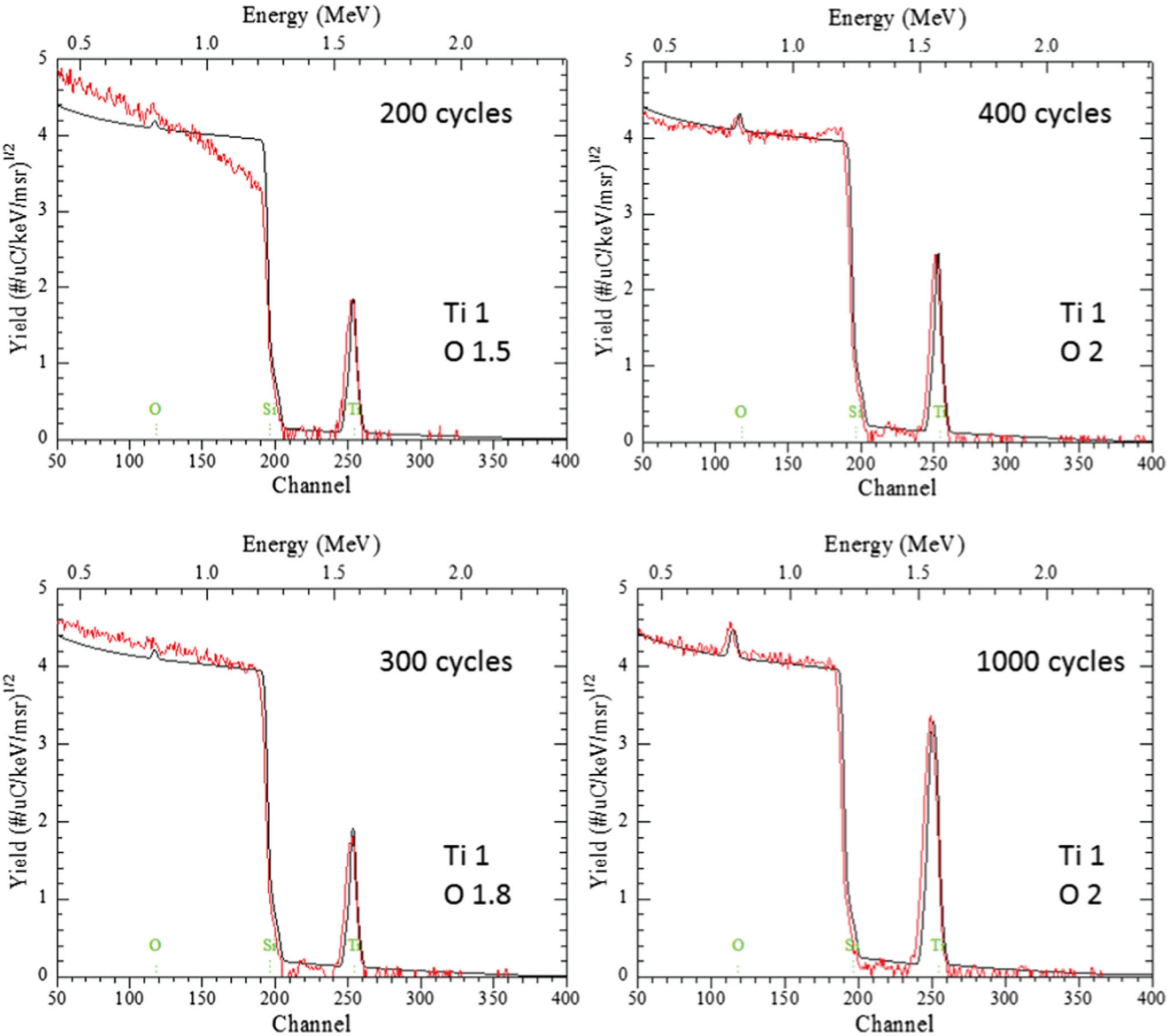

Fig. 12 Experimental and simulated RBS spectra of TiO_2 deposited at 200, 300, 400, and 1000 cycles for a process temperature of 250 °C. Simulated RBS spectra are represented by continuous line

4 Conclusion

This paper presents a thorough investigation concerning the effect of process temperature and reaction cycle number on the crystallinity/film orientation, chemical composition, and surface roughness of TiO_2 films grown on Si(100) by thermal ALD from $TiCl_4$ and H_2O precursors. Additionally, time evolution monitoring of gas phase species HCl and H_2O during ALD process was performed for different process temperatures in order to better explain the material results. A major point to be emphasized is that the GPC does not correlate well with film crystallinity and surface roughness for the evaluated process parameters. Basically, the film crystallinity relies solely on grain growth kinetics of the material. This occurs due to higher HCl by-product content during each purge step. To better explain the evolution of film crystallinity with process temperature, measurements of the film surface roughness were made, and a similar behavior was found when both parameters, crystallinity and surface roughness, are compared. Still on the effect of process temperature, mass spectrometry analysis of HCl^+ species with deposition time evidenced that the anomalous effect of GPC occurs due to precursor overlapping during lower purge time steps and that HCl^+ species is a good indicator of the behavior of GPC when the process temperature is varied.

Furthermore, in our films deposited at variable reaction cycle number, the evolution of film thickness and its elemental composition is accompanied by an amorphous structure with

near stoichiometric TiO_{2-x}, where only from 400 cycles, the TiO_2 film becomes fully stoichiometric. At this cycle value, GIXRD indicates the formation of A(101) orientation.

Finally, it can be pointed out that TiO_2 thin films with a high degree of crystallinity in pure anatase phase could be synthesized with different surface roughness by only modifying the process temperature and reaction cycle number. These films are interesting for applications in photoelectrochemical cells, and an extension of this work is the synthesis of this material on other substrate materials such as transparent conducting oxide (TCO).

Acknowledgments The authors are grateful for Tiago Fiorini da Silva from Physics Department - USP for RBS measurements and Carlos Kazuo Inoki from Brazilian Nanotechnology National Laboratory - LNNano/LNLS for TEM measurements. The financial support of Brazilian agency program FAPESP/MCT/CNPq-PRONEX (grant no. 11/50773-0), FAPESP (grant no. 15/05956-0), CNPq (grant no. 305496/2012-3 and 446545/2014-7), and Brazilian Space Agency (AEB/Uniespaço) are also strongly acknowledged.

References

1. B. Agnarsson, F. Magnus, T.K. Tryggvason, A.S. Ingason, K. Leosson, S. Olafsson, J.T. Gudmundsson, Rutile TiO_2 thin films grown by reactive high power impulse magnetron sputtering. Thin Solid Films **545**, 445–450 (2013)
2. M.A. Henderson, A surface science perspective on TiO_2 photocatalysis. Surf. Sci. Rep. **66**, 185–297 (2011)
3. U. Diebold, The surface science of titanium dioxide. Surf. Sci. Rep. **48**, 53–229 (2003)
4. J. Ângelo, L. Andrade, L.M. Madeira, A. Mendes, An overview of photocatalysis phenomena applied to NO_x abatement. J. Environ. Manage. **129**, 522–539 (2013)
5. Z.F. Yin, L. Wu, H.G. Yang, Y.H. Su, Recent progress in biomedical applications of titanium dioxide. Phys. Chem. Chem. Phys. **15**, 4844–4858 (2013)
6. V.-S. Dang, H. Parala, J.H. Kim, K. Xu, N.B. Srinivasan, E. Edengeiser, M. Havenith, A.D. Wieck, T. de los Arcos, R.A. Fischer, A. Devi, Electrical and optical properties of TiO_2 thin films prepared by plasma-enhanced atomic layer deposition. Phys. Status Solid A **211**(2), 416–424 (2014)
7. M.D. Wiggins, M.C. Nelson, C.R. Aita, Phase development in sputter deposited titanium dioxide. J. Vac. Sci. Technol. A **14**(3), 772–776 (1996)
8. J. Lee, S.J. Lee, W.B. Han, H. Jeon, J. Park, W. Jang, C.S. Yoon, H. Jeon, Deposition temperature dependence of titanium oxide thin films grown by remote-plasma atomic layer deposition. Phys. Status Solid A **210**(2), 276–284 (2013)
9. V. Pore, *Atomic Layer Deposition and Photocatalytic Properties of Titanium Dioxide Thin Films, Master Dissertation*, University of Helsinki, Finland (2010), p. 89
10. S.-Y. Lee, S.-J. Park, TiO_2 photocatalyst for water treatment applications. J. Ind. Eng. Chem. **19**, 1761–1769 (2013)
11. E. Serrano, G. Rus, J. Garcıa-Martınez, Nanotechnology for sustainable energy. Renew. Sustain. Energy Rev. **13**, 2373–2384 (2009)
12. R.S. Pessoa, M.A. Fraga, L.V. Santos, M. Massi, H.S. Maciel, Nanostructured thin films based on TiO_2 and/or SiC for use in photoelectrochemical cells: a review of the material characteristics, synthesis and recent applications. Mater. Sci. Semicond Process **29**, 56–68 (2015)
13. P. Kajitvichyanukul, J. Ananpattarachai, S. Pongpom, Sol–gel preparation and properties study of TiO2 thin film for photocatalytic reduction of chromium(VI) in photocatalysis process. Sci. Technol. Adv. Mater. **6**, 352–358 (2005)
14. X. Chen, S.S. Mao, Titanium dioxide nanomaterials: synthesis, properties, modifications, and applications. Chem. Rev. **107**(7), 2891–2959 (2007)
15. D. Regonini, C.R. Bowen, A. Jaroenworaluck, R. Stevens, A review of growth mechanism, structure and crystallinity of anodized TiO_2 nanotubes. Mater. Sci. Eng. R **74**(12), 377–406 (2013)
16. S. Venkatachalam, H. Hayashi, T. Ebina and H. Nanjo, *Preparation and Characterization of Nanostructured TiO_2 Thin Films by Hydrothermal and Anodization Methods, Optoelectronics, Advanced Materials and Devices*, Prof. Sergei Pyshkin (Ed.), ISBN: 978-953-51-0922-8, InTech (2013)
17. H. Toku, R.S. Pessoa, H.S. Maciel, M. Massi, U.A. Mengui, The effect of oxygen concentration on the low temperature deposition of TiO_2 thin films. Surf. Coat. Technol. **202**, 2126–2131 (2008)
18. T. Sakae, L. Miao, W. Wunderlich, M. Tanemura, Y. Mori, S. Toh, K. Kaneko, Fabrication and characterization of anatase/rutile–TiO_2 thin films by magnetron sputtering: a review. Sci. Technol. Adv. Mater. **6**, 11–17 (2005)
19. S.S. Huang, J.S. Chen, Comparison of the characteristics of TiO_2 films prepared by low-pressure and plasma-enhanced chemical vapor deposition. J Mater Sci Mater Electron **13**, 77–81 (2002)
20. F. Maury, J. Mungkalasiri, Chemical vapor deposition of TiO_2 for photocatalytic applications and biocidal surfaces. Key Eng. Mater. **415**, 1–4 (2009)
21. A.K. Chandiran, P. Comte, R. Humphry-Baker, F. Kessler, C. Yi, M.K. Nazeeruddin, M. Grätzel, Evaluating the critical thickness of TiO_2 layer on insulating mesoporous templates for efficient current collection in Dye-sensitized solar cells. Adv. Funct. Mater. **23**, 2775–2781 (2013)
22. J.A. van Delft, D. Garcia-Alonso, W.M.M. Kessels, Atomic layer deposition for photovoltaics: applications and prospects for solar cell manufacturing. Semicond. Sci. Technol. **27**, 074002 (2012)
23. R.L. Puurunen, Surface chemistry of atomic layer deposition: a case study for the trimethylaluminum/water process. J. Appl. Phys. **97**, 121301 (2005)
24. V. Miikkulainen, M. Leskelä, M. Ritala, R.L. Puurunen, Crystallinity of inorganic films grown by atomic layer deposition: overview and general trends. J. Appl. Phys. **113**, 021301 (2013)
25. J. Leem, I. Park, Y. Li, W. Zhou, Z. Jin, S. Shin, Y.-S. Min, Role of HCl in atomic layer deposition of TiO_2 thin films from titanium tetrachloride and water. Bull. Korean Chem. Soc. **35**(4), 1195–1201 (2014)
26. R.P. Chaukulkar, S. Agarwal, Atomic layer deposition of titanium dioxide using titanium tetrachloride and titanium tetraisopropoxide as precursors. J. Vac. Sci. Technol. A **31**(3), 031509 (2013)
27. T. Blanquart, *Atomic layer deposition of groups 4 and 5 transition metal oxide thin films: focus on heteroleptic precursors, Master Dissertation*, University of Helsinki, Finland (2013), p. 68
28. J. Aarik, A. Aidla, V. Sammelselg, T. Uustare, M. Ritala, M. Leskela, Characterization of titanium dioxide atomic layer growth from titanium ethoxide and water. Thin Solid Films **370**, 163–172 (2000)
29. M. Ritala, M. Leskelä, E. Nykänen, P. Soininen, L. Niinistö, Growth of titanium dioxide thin films by atomic layer epitaxy. Thin Solid Films **225**, 288–295 (1993)
30. M. Ritala, M. Leskelä, L.-S. Johansson, L. Niinistö, Atomic force microscopy study of titanium dioxide thin films grown by atomic layer epitaxy. Thin Solid Films **228**, 32–35 (1993)

31. J. Aarik, A. Aidla, T. Uustare, V. Sammelselg, Morphology and structure of TiO_2 thin films grown by atomic layer deposition. J. Cryst. Growth **148**, 268–275 (1995)
32. J. Aarik, A. Aidla, V. Sammelselg, H. Siimon, T. Uustare, Control of thin film structure by reactant pressure in atomic layer deposition of TiO_2. J. Crystal Growth **169**, 496–502 (1996)
33. J. Aarik, A. Aidla, A.-A. Kiisler, T. Uustare, V. Sammelselg, Effect of crystal structure on optical properties of TiO_2 films grown by atomic layer deposition. Thin Solid Films **305**, 270–273 (1997)
34. V. Sammelselg, A. Rosental, A. Tarre, L. Niinisto, K. Heiskanen, K. Ilmonen, L.-S. Johansson, T. Uustare, TiO_2 thin films by atomic layer deposition: a case of uneven growth at low temperature. Appl. Surf. Sci. **134**, 78–86 (1998)
35. J. Aarik, A. Aidla, H. Mändar, V. Sammelselg, Anomalous effect of temperature on atomic layer deposition of titanium dioxide. J. Crystal Growth **220**, 531–537 (2000)
36. J. Aarik, A. Aidla, H. Mändar, T. Uustare, Atomic layer deposition of titanium dioxide from $TiCl_4$ and H_2O: investigation of growth mechanism. Appl. Surf. Sci. **172**, 148–158 (2001)
37. J. Aarik, A. Aidla, H. Mandar, T. Uustare, M. Schuisky, A. Harsta, Atomic layer growth of epitaxial TiO_2 thin films from $TiCl_4$ and H_2O on α-Al_2O_3 substrates. J. Crystal Growth **242**, 189–198 (2002)
38. D.R.G. Mitchell, D.J. Attard, G. Triani, Transmission electron microscopy studies of atomic layer deposition TiO_2 films grown on silicon. Thin Solid Films **441**, 85–95 (2003)
39. K.S. Finnie, G. Triani, K.T. Short, D.R.G. Mitchell, D.J. Attard, J.R. Bartlett, C.J. Barbé, Influence of Si(100) surface pretreatment on the morphology of TiO_2 films grown by atomic layer deposition. Thin Solid Films **440**, 109–116 (2003)
40. A. Niilisk, M. Moppel, M. Pärs, I. Sildos, T. Jantson, T. Avarmaa, R. Jaaniso, J. Aarik, Structural study of TiO_2 thin films by micro-Raman spectroscopy. Cent. Eur. J. Phys. **4**(1), 105–116 (2006)
41. H.-E. Cheng, C.-C. Chen, Morphological and photoelectrochemical properties of ALD TiO_2 films. J. Electrochem. Soc. **155**(9), D604–D607 (2008)
42. R.L. Puurunen, T. Sajavaara, E. Santala, V. Miikkulainen, T. Saukkonen, M. Laitinen, M. Leskelä, Controlling the crystallinity and roughness of atomic layer deposited titanium dioxide thin films. J. Nanosci. Nanotechnol. **11**, 8101–8107 (2011)
43. L. Aarik, T. Arroval, R. Rammula, H. Mändar, V. Sammelselg, J. Aarik, Atomic layer deposition of TiO_2 from $TiCl_4$ and O_3. Thin Solid Films **542**, 100–107 (2013)
44. M. Mayer, AIP Conf. Proc. 475 (1999) 541; SIMNRA (Simulation Program for the Analysis of NRA, RBS and ERDA) developed by M. Mayer; http://home.rzg.mpg.de/~mam/.
45. D. Nečas, P. Klapetek, Gwyddion: an open-source software for SPM data analysis. Cent. Eur. J. Phys. **10**(1), 181–188 (2012)
46. R.L. Puurunen, Growth per cycle in atomic layer deposition: a theoretical model. Chem. Vap. Depos. **9**(5), 249–257 (2003)
47. R.L. Puurunen, Surface chemistry of atomic layer deposition: a case study for the trimethylaluminum/water process. J. Appl. Phys. **97**, 121301 (2005)
48. K.-E. Elers, T. Blomberg, M. Peussa, B. Aitchison, S. Haukka, S. Marcus, Film uniformity in atomic layer deposition. Chem. Vap. Depos. **12**, 13–24 (2006)
49. M.E. Mrose, B. Post, S. Weissmann, H.F. McMurdie, M.C. Morris, W.F. McClune (eds.), *Powder Diffraction Data, Joint Committee on Powder Diffraction Data Standards*, Swarthmore, PA, cards 16-617, 21-1272 and 21-1276 (1976).
50. J. Shi, Z. Li, A. Kvit, S. Krylyuk, A.V. Davydov, X. Wang, Electron microscopy observation of TiO_2 nanocrystal evolution in high-temperature atomic layer deposition. Nano Lett. **13**, 5727–5734 (2013)
51. M. Ritala, M. Leskela, L. Niinistö, T. Prohaska, G. Friedbacher, M. Grasserbauer, Development of crystallinity and morphology in hafnium dioxide thin films grown by atomic layer epitaxy. Thin Solid Films **250**, 72–80 (1994)
52. V. Sammelselg, J. Aarik, A. Aidla, A. Kasikov, E. Heikinheimo, M. Peussa, L. Niinisto, Composition and thickness determination of thin oxide films: comparison of different programs and methods. J. Anal. At. Spectrom. **14**, 523–527 (1999)
53. A. Sinha, D.W. Hess, C.L. Henderson, Area selective atomic layer deposition of titanium dioxide: effect of precursor chemistry. J. Vac. Sci. Technol. B **24**, 2523–2532 (2006)
54. G. Triani, J.A. Campbell, P.J. Evans, J. Davis, B.A. Latella, R.P. Burford, Low temperature atomic layer deposition of titania thin films. Thin Solid Films **518**, 3182–3189 (2010)